

# Geometric phases in open tripod systems

Ditte Møller,\* Lars Bojer Madsen, and Klaus Mølmer  
*Lundbeck Foundation Theoretical Center for Quantum System Research,  
Department of Physics and Astronomy, University of Aarhus, DK-8000, Denmark.*  
(Dated: March 24, 2022)

We first consider stimulated Raman adiabatic passages (STIRAP) in a closed four-level tripod system. In this case, the adiabatic eigenstates of the system acquire real geometric phases. When the system is open and subject to decoherence they acquire complex geometric phases that we determine by a Monte Carlo wave function approach. We calculate the geometric phases and the state evolution in the closed as well as in the open system cases and describe the deviation between these in terms of the phases acquired. When the system is closed, the adiabatic evolution implements a Hadamard gate. The open system implements an imperfect gate and hence has a fidelity below unity. We express this fidelity in terms of the acquired geometric phases.

PACS numbers: 03.67.Lx, 03.65.Vf, 03.65.Yz

## I. INTRODUCTION

Each eigenstate of a non-degenerate quantum system that evolves adiabatically in time acquires a well-defined phase in addition to the usual dynamic phase. The former is called the geometric phase because it depends on the path traversed in Hilbert space [1]. With the current interest in quantum information and computation, the geometric phase has received new attention because it is expected to be robust against some sources of decoherence [2, 3, 4, 5] and hence useful, e.g., for creation of quantum gates. To study its robustness under decoherence it is essential to generalize the concept of geometric phase to open quantum systems. Various proposals have been made [6, 7] and they all point to the problem that phase information tends to be lost when the system is open and decoheres, e.g., due to spontaneous emission.

The full system including decoherence can still be described, for example, by the density matrix approach, which predicts the relative phases between the involved basis states, but the information about the phases acquired by each eigenstate is not available nor is the information about the geometric or dynamic nature of the phase. In this work we are interested in the phase dynamics of the states of the physical system when the system is subject to decoherence. To this end we consider the Monte Carlo wave function (MCWF) approach [8, 9]. We follow each wave function trajectory and calculate the complex geometric phases that are acquired by the adiabatic eigenstates. The MCWF approach has the advantage that we gain information about the evolution of the single trajectories and the dynamic or geometric nature of the phases. Not surprisingly, on average the trajectories reproduce the density matrix result. We show how the evolution of the open system can be described by adiabatic eigenstates that acquire complex geometric phases and we discuss the deviation from the closed system case

in terms of the phases acquired. We consider a tripod system with three laser fields applied and present a full calculation of the adiabatic evolution of the wave function of the system. The adiabatic evolution considered consist of a sequence of stimulated Raman adiabatic passages (STIRAP)[10] and implements the Hadamard gate. We quantify the effect of decoherence in terms of the fidelity of this gate and identify the role of the complex geometric phases.

The paper is organized as follows. In Sec. II we review the theory of geometric phases, we explain their appearance in STIRAP processes and present the tripod system. In Sec. III we present calculations for the closed system and in Sec. IV we derive the full solution for the evolution of the open system evolution and calculate the fidelity of the Hadamard gate. Sec. V concludes.

## II. BACKGROUND

### A. Geometric phase

The adiabatic theorem states that for a given set of instantaneous eigenstates,  $\psi_n(t)$ , and eigenenergies,  $E_n(t)$ , of a time-dependent Hamiltonian, there is no population transfer between the eigenstates if these vary slowly compared with the energy difference between eigenstates [11]

$$\left| \frac{\partial \psi_n}{\partial t} \right| \ll \frac{|E_n - E_m|}{\hbar}. \quad (1)$$

In this adiabatic regime the eigenstates do not only acquire a dynamic phase,  $\vartheta_n = \int_{t_i}^{t_f} E_n(t')/\hbar dt'$ , but also a geometric phase,  $\gamma_n$

$$\Psi(0) = \sum_n c_n(0) \psi_n(0) \xrightarrow{ad} \Psi(t) = \sum_n c_n(0) e^{i(\vartheta_n + \gamma_n)} \psi_n(t), \quad (2)$$

\*Electronic address: dittem@phys.au.dk

where the geometric part of the phase can be calculated directly from the eigenstates [1],

$$\gamma_n = i \int_{\bar{R}_i}^{\bar{R}_f} \langle \psi_n(\bar{R}) | \nabla_{\bar{R}} | \psi_n(\bar{R}) \rangle \cdot d\bar{R}. \quad (3)$$

Here  $\bar{R}$  are time-dependent parameters of the Hamiltonian, and the geometric phase becomes an integral in the space of these parameters (See Eq. (7) below for a specific example).

### B. STIRAP in lambda system

STIRAP is an efficient, adiabatic process for population transfer in three-level systems. In the method two laser fields are applied to the atomic lambda system [see Fig. 1(a)] [10, 12, 13, 14, 15, 16, 17, 18]. The instantaneous adiabatic dressed states for this system are two bright states and one dark state. The explicit form of the dark state ( $|D\rangle$ ) with zero energy eigenvalue,  $\omega^D = 0$ , reads

$$\begin{aligned} |D\rangle &= \frac{\Omega_2}{\sqrt{|\Omega_0|^2 + |\Omega_2|^2}} |0\rangle - \frac{\Omega_0}{\sqrt{|\Omega_0|^2 + |\Omega_2|^2}} |2\rangle \\ &= \cos\theta |0\rangle - \sin\theta e^{i\varphi_2} |2\rangle, \end{aligned} \quad (4)$$

where  $\Omega_0$  and  $\Omega_2$  are Rabi frequencies (see Fig. 1),  $\tan\theta = |\Omega_0|/|\Omega_2|$  and  $\varphi_2$  is the time-dependent phase difference between the two laser fields. The real amplitudes of the fields,  $A_0(t)$  and  $A_2(t)$  are time-dependent and the Rabi frequencies explicitly read

$$\begin{aligned} \Omega_0(t) &= A_0(t), \\ \Omega_2(t) &= A_2(t)e^{-i\varphi_2(t)}. \end{aligned} \quad (5)$$

The pulses are modeled by  $\sin^2$ -pulses with different amplitudes

$$A_j(t) = \begin{cases} A_{\max,j} \sin^2\left(\frac{\pi(t-t_{sj})}{2\tau}\right) & \text{if } t_{sj} < t < t_{sj} + 2\tau \\ 0 & \text{otherwise} \end{cases}, \quad (6)$$

where  $t_{sj}$  is the instant of time when the pulse starts and  $\tau$  the FWHM. With all population initially in the  $|0\rangle$ -state and only  $\Omega_2$  applied the system is in this dark state. Now, adiabatically increasing  $\Omega_0$  and decreasing  $\Omega_2$  causes population transfer from  $|0\rangle$  to  $|2\rangle$ , while all population remains in  $|D\rangle$  of Eq. (4). This implies that the excited state,  $|e\rangle$  is never populated and hence no population is lost due to spontaneous emission.

STIRAP is well-suited for studying geometric phases, because no dynamic phase is acquired,  $\omega^D = 0$ . The geometric phase is calculated by Eq. (3) with  $\bar{R} = (\theta, \varphi_2)$ ,

$$\gamma_D = i \int_{\bar{R}_i}^{\bar{R}_f} \langle D | \nabla_{\bar{R}} | D \rangle \cdot d\bar{R} = - \int_{t_i}^{t_f} \dot{\varphi}_2 \sin^2\theta dt. \quad (7)$$

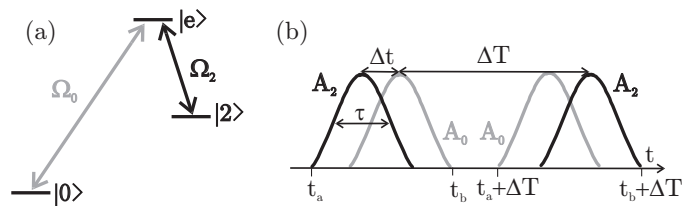


FIG. 1: (a) Three-level lambda system with two laser fields applied with Rabi frequencies  $\Omega_0$  and  $\Omega_2$ . (b) Pulse sequence consisting of two STIRAP processes separated by  $\Delta T$  in time. The first set of pulses transfers population from  $|0\rangle$  to  $|2\rangle$ , while the second set transfers it back. We show the real amplitudes,  $A_0$  and  $A_2$  of the Rabi frequencies  $\Omega_0$  and  $\Omega_2$  as defined in Eq. (5). With this pulse sequence  $\sin\theta = \Omega_0/(\sqrt{|\Omega_0|^2 + |\Omega_2|^2})$  is zero before the first pair of pulses arrive, one in between the two processes and zero after the second pair of pulses. The FWHM of each pulse is  $\tau$  and the delay between pulses within one process is  $\Delta t$ .

To obtain a non-zero  $\gamma_D$ , the phase difference between the two laser fields,  $\varphi_2$ , should be controlled and have a time-dependence with non-vanishing  $\dot{\varphi}_2$ . In order to be able to control the actual value of  $\gamma_D$  we require that  $\sin^2\theta = 0$  before and after the pulse sequence, ensuring that only during the sequence a geometric phase is acquired. As stated in Eq. (4)  $\sin^2\theta = |\Omega_0|^2/(|\Omega_0|^2 + |\Omega_2|^2)$ , which implies that during one STIRAP process  $\sin^2\theta$  is increased from zero to one. Applying a second STIRAP process, where  $\Omega_0$  is decreased while  $\Omega_2$  is increased, decreases  $\sin^2\theta$  from one to zero. This second process transfers the population from  $|2\rangle$  back to  $|0\rangle$ . The whole pulse sequence is shown in Fig. 1(b) and after this sequence the system ends up in

$$|D\rangle = e^{i\gamma_D} |0\rangle, \quad (8)$$

where  $\gamma_D$  is calculated from Eq. (7) with  $t_i = t_a$  and  $t_f = t_b + \Delta T$  as defined in Fig. 1(b).

### C. STIRAP in tripod system

In the lambda system described above the geometric phase acquired by the dark state,  $|D\rangle$  is a collective phase on the two atomic states,  $|0\rangle$  and  $|2\rangle$ . We now turn to the tripod system shown in Fig. 2(a). This system has the advantage that two dark states are populated and these acquire different geometric phases leading to relative phases between the atomic states as well as changes in their population due to changes in the interference of the two dark states. In the tripod system we can therefore calculate the geometric phase and see how it affects the measurable populations and relative phases between the atomic states. The tripod system further constitute a system, where a universal set of quantum gates can be implemented (see, e.g., [19] and references therein). The level structure consists of three lower states ( $|0\rangle$ ,  $|1\rangle$  and  $|2\rangle$ ) coupled to an excited state,  $|e\rangle$ , with

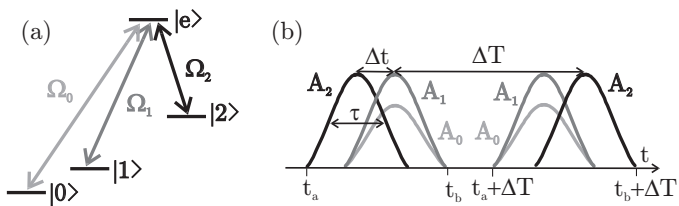


FIG. 2: (a) Four-level tripod system with three laser fields applied with Rabi frequencies  $\Omega_0$ ,  $\Omega_1$ ,  $\Omega_2$ . (b) Pulse sequence consisting of two STIRAP processes separated by  $\Delta T$  in time. The first set of pulses transfers population from  $\{|0\rangle, |1\rangle\}$  to  $|2\rangle$ , while the second set transfers it back. We show the real amplitudes,  $A_0$ ,  $A_1$  and  $A_2$  of the Rabi frequencies  $\Omega_0$ ,  $\Omega_1$  and  $\Omega_2$  as defined in Eq. (9). The FWHM of each pulse is  $\tau$  and the delay between pulses within one process is  $\Delta t$ .

three laser fields. These have Rabi frequencies  $\Omega_0$ ,  $\Omega_1$  and  $\Omega_2$ , respectively, and for simplicity we assume that they are all on resonance. We restrict ourselves to the case where the relative phase between  $\Omega_0$  and  $\Omega_1$ ,  $\varphi_{01}$ , is time-independent while the phase of  $\Omega_2$ ,  $\varphi_2(t)$ , is time-dependent. The real amplitudes of all fields,  $A_0(t)$ ,  $A_1(t)$  and  $A_2(t)$  are time-dependent and the Rabi frequencies explicitly read

$$\begin{aligned}\Omega_0(t) &= A_0(t), \\ \Omega_1(t) &= A_1(t)e^{-i\varphi_{01}}, \\ \Omega_2(t) &= A_2(t)e^{-i\varphi_2(t)}.\end{aligned}\quad (9)$$

The pulses are as in the lambda-system case modeled by the  $\sin^2$ -pulses in Eq. (6). When we apply the pulse sequence shown in Fig. 2(b), the STIRAP process transfers part of the population from  $|0\rangle$  and  $|1\rangle$  to  $|2\rangle$  and back. During this process geometric phases are acquired. Calculations of the evolution of the system is presented in

Sec. III for a closed system and in Sec. IV for an open system.

### III. CLOSED SYSTEM

In the rotating wave approximation, and with Rabi frequencies as defined in Eq. (9), we derive the Hamiltonian

$$H(t) = \frac{\hbar}{2} \begin{bmatrix} 0 & 0 & A_0(t) & 0 \\ 0 & 0 & A_1(t)e^{i\varphi_{01}} & 0 \\ A_0(t) & A_1(t)e^{-i\varphi_{01}} & 0 & A_2(t)e^{-i\varphi_2(t)} \\ 0 & 0 & A_2(t)e^{i\varphi_2(t)} & 0 \end{bmatrix} \quad (10)$$

expressed in the  $\{|0\rangle, |1\rangle, |e\rangle, |2\rangle\}$  basis. We parameterize the complex Rabi frequencies as

$$\Omega_0(t) = \sin \theta_{01} \sqrt{A_0(t)^2 + A_1(t)^2}, \quad (11)$$

$$\Omega_1(t) = \cos \theta_{01} \sqrt{A_0(t)^2 + A_1(t)^2} e^{-i\varphi_{01}}, \quad (12)$$

$$\Omega_2(t) = \cos \theta_H(t) \sqrt{A_0(t)^2 + A_1(t)^2 + A_2(t)^2} e^{-i\varphi_2(t)}, \quad (13)$$

where the two angles are defined as

$$\tan \theta_{01} = A_0(t)/A_1(t), \quad (14)$$

$$\tan \theta_H(t) = \sqrt{A_0^2(t) + A_1^2(t)}/A_2(t). \quad (15)$$

A diagonalization of Eq. (10) gives the four energy eigenvalues

$$\omega^\pm = \pm \frac{1}{2} \sqrt{A_0^2 + A_1^2 + A_2^2}, \quad \omega^{D_i} = 0 \quad (i = 1, 2), \quad (16)$$

and eigenvectors

$$\begin{aligned}|+\rangle &= \frac{1}{\sqrt{2}} \left[ \sin \theta_H(t) (\sin \theta_{01} |0\rangle + \cos \theta_{01} e^{i\varphi_{01}} |1\rangle) - |e\rangle + \cos \theta_H(t) e^{i\varphi_2(t)} |2\rangle \right], \\ |-\rangle &= \frac{1}{\sqrt{2}} \left[ \sin \theta_H(t) (\sin \theta_{01} |0\rangle + \cos \theta_{01} e^{i\varphi_{01}} |1\rangle) + |e\rangle + \cos \theta_H(t) e^{i\varphi_2(t)} |2\rangle \right], \\ |D_1\rangle &= -\cos \theta_H(t) (\sin \theta_{01} |0\rangle + \cos \theta_{01} e^{i\varphi_{01}} |1\rangle) + \sin \theta_H(t) e^{i\varphi_2(t)} |2\rangle, \\ |D_2\rangle &= \cos \theta_{01} |0\rangle - \sin \theta_{01} e^{i\varphi_{01}} |1\rangle.\end{aligned}\quad (17)$$

We assume that we start out in a superposition of the two dark eigenstates at time  $t_i$

$$|D(t_i)\rangle = C_{D_1}(t_i)|D_1(t_i)\rangle + C_{D_2}(t_i)|D_2(t_i)\rangle, \quad (18)$$

and that the evolution is adiabatic. Then the population stays within the space spanned by the two dark states

and at later times the wave function is given by

$$|D(t)\rangle = C_{D_1}(t)|D_1(t)\rangle + C_{D_2}(t)|D_2(t)\rangle. \quad (19)$$

In order to determine the time evolution of the coefficients  $\{C_{D_1}(t), C_{D_2}(t)\}$  we follow Refs. [12, 20]. Inserting Eq. (19) into the time-dependent Schrödinger equation yields two coupled differential equations that can

readily be solved and we find the very simple evolution

$$\begin{aligned} C_{D_1}(t) &= e^{i\gamma_{D_1}} C_{D_1}(t_i), \\ C_{D_2}(t) &= C_{D_2}(t_i). \end{aligned} \quad (20)$$

Here the phase

$$\gamma_{D_1} = - \int_{t_i}^t \dot{\varphi}_2 \sin^2 \theta_H dt', \quad (21)$$

acquired by  $|D_1\rangle$  is purely geometric because the dark states do not acquire any dynamic phases,  $\omega^{D_i} = 0$ . Since no population is transferred between the two dark states the geometric phase could also be calculated using Eq. (3). This approach was used in [19].

STIRAP (Sec. II B) ensures control of the geometric phases. The exact pulse sequence is shown in Fig. 2(b). The first set of pulses transfers population partially from  $|0\rangle$  and  $|1\rangle$  to  $|2\rangle$  while the second transfers all population back to  $|0\rangle$  and  $|1\rangle$ . The amplitudes of  $\Omega_0$  and  $\Omega_1$  are

such that  $\theta_{01}$  is kept constant. The amplitude of  $\Omega_2$  is  $A_{\max,2} = \sqrt{A_{\max,0}^2 + A_{\max,1}^2}$  and the pulse of  $\Omega_2$  is delayed with respect to the pulses of  $\Omega_0$  and  $\Omega_1$  and hence  $\sin \theta_H(t)$  is varied from 0 to 1 when the first set of pulses arrive, while the second set of pulses adiabatically turns the  $\sin \theta_H(t)$  factor back to 0. After the whole pulse sequence the system ends up in the final state

$$\begin{aligned} |D(t_f)\rangle &= C_{D_1}(t_i) e^{i\gamma_{D_1}(t_f)} |D_1(t_f)\rangle + C_{D_2}(t_i) |D_2(t_f)\rangle \\ &= [-\sin \theta_{01} C_{D_1}(t_i) e^{i\gamma_{D_1}} + \cos \theta_{01} C_{D_2}(t_i)] |0\rangle \\ &\quad + [-\cos \theta_{01} C_{D_1}(t_i) e^{i\gamma_{D_1}} + \sin \theta_{01} C_{D_2}(t_i)] |1\rangle, \end{aligned} \quad (22)$$

where we have used Eq. (17) in the second line. In the  $\{|0\rangle, |1\rangle\}$ -basis, an arbitrary initial state  $|\psi_i\rangle = a_i|0\rangle + b_i|1\rangle$  is transferred by the unitary matrix  $U$  to a final state  $|\psi_f\rangle = U|\psi_i\rangle = a_f|0\rangle + b_f|1\rangle$  with

$$U = \begin{bmatrix} \cos^2 \theta_{01} + e^{i\gamma_{D_1}} \sin^2 \theta_{01} & \cos \theta_{01} \sin \theta_{01} e^{-i\varphi_{01}} (e^{i\gamma_{D_1}} - 1) \\ \cos \theta_{01} \sin \theta_{01} e^{i\varphi_{01}} (e^{i\gamma_{D_1}} - 1) & \sin^2 \theta_{01} + e^{i\gamma_{D_1}} \cos^2 \theta_{01} \end{bmatrix}. \quad (23)$$

By carefully adjusting the amplitudes and phases of the laser fields, the values of  $\theta_{01}$ ,  $\varphi_{01}$  and  $\gamma_{D_1}$  can be controlled and thus generate rotations in the  $\{|0\rangle, |1\rangle\}$ -basis. We note that  $U$  is the identity when no geometric phase is acquired,  $\gamma_{D_1} = 0$ . As a special case  $\theta_{01} = \frac{\pi}{8}$ ,  $\varphi_{01} = \pi$  and  $\gamma_{D_1} = -\pi$  implement a Hadamard gate

$$U = \frac{1}{\sqrt{2}} \begin{bmatrix} 1 & 1 \\ 1 & -1 \end{bmatrix}. \quad (24)$$

The value  $\theta_{01} = \frac{\pi}{8}$  is obtained by choosing  $A_{\max,0} = A_{\max,1}(\sqrt{2} - 1)$ ,  $A_{\max,2} = \sqrt{A_{\max,0}^2 + A_{\max,1}^2}$  and  $\varphi_2 = t/\tau$ ,  $\Delta T/\tau = \pi$  assures  $\gamma_{D_1} = -\pi$ . All simulations presented throughout this work will use these parameters and the initial state  $|\psi_i\rangle = |0\rangle$  which is transferred to the final state  $|\psi_f\rangle = U|\psi_i\rangle = (|0\rangle + |1\rangle)/\sqrt{2}$  in the closed system case.

#### IV. OPEN SYSTEM

We use STIRAP to transfer population among  $|0\rangle$ ,  $|1\rangle$  and  $|2\rangle$ , while keeping the population in the excited state  $|e\rangle$  negligible. Decoherence due to spontaneous emission will therefore have very little effect, while dephasing caused by, e.g., collisions or phase fluctuations of the laser fields, will influence the evolution. The evolution of the open system can be found by solving the Lindblad

master equation [21],

$$\dot{\rho} = -\frac{i}{\hbar} [H, \rho] - \frac{1}{2} \sum_m (C_m^\dagger C_m \rho + \rho C_m^\dagger C_m) + \sum_m C_m \rho C_m^\dagger, \quad (25)$$

where  $H$  is the Hamiltonian for the closed system and the decoherence is described by the Lindblad operators,  $C_m$ . The Lindblad master equation results in an ensemble average of the evolution, but does not reveal a clear distinction between the geometric and dynamic phases. We wish to follow the evolution of the wave functions, the acquired geometric and dynamic phases and how these affect the relative phases between and the population in the atomic states. Towards this end we use the quantum jump approach, where the wave function is evolved stochastically [8, 9]. For a small timestep  $\Delta t$  the evolution of the wave function is described as either a jump to  $C_m|\psi(t)\rangle$  or by a no-jump evolution with the non-Hermitian Hamiltonian  $\tilde{H} = H + H'$ , where  $H' = -i\hbar/2 \sum_m C_m^\dagger C_m$ . After a timestep with either the jump or the no-jump evolution the wave function is normalized. The probability for a jump to  $C_m|\psi(t)\rangle$  in  $\Delta t$  is  $P_m(t) = \Delta t \langle \psi(t) | C_m^\dagger C_m | \psi(t) \rangle$ . For the method to be valid the total probability for a jump in  $\Delta t$  has to be small,  $P = \sum_m P_m \ll 1$ . The method leads to many different traces, which on average reproduce the density matrix. For further details see, e.g., Refs. [8, 9].

We model the dephasing by a single Lindblad operator,

$C_0 = \sqrt{2\Gamma_0}|0\rangle\langle 0|$ , yielding the master equation

$$\dot{\rho} = -\frac{i}{\hbar}[H, \rho] - \begin{bmatrix} 0 & \Gamma_0\rho_{01} & \Gamma_0\rho_{0e} & \Gamma_0\rho_{02} \\ \Gamma_0\rho_{10} & 0 & 0 & 0 \\ \Gamma_0\rho_{e0} & 0 & 0 & 0 \\ \Gamma_0\rho_{20} & 0 & 0 & 0 \end{bmatrix}. \quad (26)$$

Given  $C_0$  we can calculate the no jump evolution with  $\tilde{H}$  (Sec. IV A) as well as the jump traces (Sec. IV B), where the system is projected onto the state  $C_m|\psi(t_j)\rangle \propto |0\rangle$  at the instant of time  $t_j$ .

### A. Non-Hermitian no jump evolution

With the Lindblad operator  $C_0 = \sqrt{2\Gamma_0}|0\rangle\langle 0|$ ,  $H' = -i\hbar\Gamma_0|0\rangle\langle 0|$  and the non-Hermitian Hamiltonian of the

tripod system,  $\tilde{H} = H + H'$  reads

$$\tilde{H}(t) = \frac{\hbar}{2} \begin{bmatrix} -2i\Gamma_0 & 0 & A_0(t) & 0 \\ 0 & 0 & A_1(t)e^{i\varphi_{01}} & 0 \\ A_0(t) & A_1(t)e^{-i\varphi_{01}} & 0 & A_2(t)e^{-i\varphi_2(t)} \\ 0 & 0 & A_2(t)e^{i\varphi_2(t)} & 0 \end{bmatrix}. \quad (27)$$

In order to determine the time evolution of the system, we transform into the interaction picture with respect to  $H'$

$$\tilde{H}_I(t) = \frac{\hbar}{2} \begin{bmatrix} 0 & 0 & A_0(t)e^{\Gamma_0(t-t_i)} & 0 \\ 0 & 0 & A_1(t)e^{i\varphi_{01}} & 0 \\ A_0(t)e^{-\Gamma_0(t-t_i)} & A_1(t)e^{-i\varphi_{01}} & 0 & A_2(t)e^{-i\varphi_2(t)} \\ 0 & 0 & A_2(t)e^{i\varphi_2(t)} & 0 \end{bmatrix}. \quad (28)$$

The subscript  $I$  indicates that the evolution is described in the interaction picture. This Hamiltonian is non-Hermitian due to the  $\Gamma_0$ -exponents and in order to determine the geometric phases we follow the procedure of Ref. [22]. We diagonalize  $H_I$  and find the eigenvalues

$$\omega_I^\pm = \pm \frac{1}{2} \sqrt{A_0^2 + A_1^2 + A_2^2}, \quad \omega_I^{D_i} = 0 \quad (i = 1, 2), \quad (29)$$

and the right (subscript  $r$ ) and left (subscript  $l$ ) eigenvectors

$$\begin{aligned} |+_r\rangle_I &= \frac{1}{\sqrt{2}} \left[ \sin\theta_H(t)(\sin\theta_{01}e^{\Gamma_0(t-t_i)}|0\rangle + \cos\theta_{01}e^{i\varphi_{01}}|1\rangle) - |e\rangle + \cos\theta_H(t)e^{i\varphi_2(t)}|2\rangle \right], \\ |-_r\rangle_I &= \frac{1}{\sqrt{2}} \left[ \sin\theta_H(t)(\sin\theta_{01}e^{\Gamma_0(t-t_i)}|0\rangle + \cos\theta_{01}e^{i\varphi_{01}}|1\rangle) + |e\rangle + \cos\theta_H(t)e^{i\varphi_2(t)}|2\rangle \right], \\ |D_{1r}\rangle_I &= -\cos\theta_H(t)(\sin\theta_{01}e^{\Gamma_0(t-t_i)}|0\rangle + \cos\theta_{01}e^{i\varphi_{01}}|1\rangle) + \sin\theta_H(t)e^{i\varphi_2(t)}|2\rangle, \\ |D_{2r}\rangle_I &= \cos\theta_{01}e^{\Gamma_0(t-t_i)}|0\rangle - \sin\theta_{01}e^{i\varphi_{01}}|1\rangle, \\ \langle +_l| &= \frac{1}{\sqrt{2}} \left[ \sin\theta_H(t)(\sin\theta_{01}e^{-\Gamma_0(t-t_i)}\langle 0| + \cos\theta_{01}e^{-i\varphi_{01}}\langle 1|) - \langle e| + \cos\theta_H(t)e^{-i\varphi_2(t)}\langle 2| \right], \\ \langle -_l| &= \frac{1}{\sqrt{2}} \left[ \sin\theta_H(t)(\sin\theta_{01}e^{-\Gamma_0(t-t_i)}\langle 0| + \cos\theta_{01}e^{-i\varphi_{01}}\langle 1|) + \langle e| + \cos\theta_H(t)e^{-i\varphi_2(t)}\langle 2| \right], \\ \langle D_{1l}| &= -\cos\theta_H(t)(\sin\theta_{01}e^{-\Gamma_0(t-t_i)}\langle 0| + \cos\theta_{01}e^{-i\varphi_{01}}\langle 1|) + \sin\theta_H(t)e^{-i\varphi_2(t)}\langle 2|, \\ \langle D_{2l}| &= \cos\theta_{01}e^{-\Gamma_0(t-t_i)}\langle 0| - \sin\theta_{01}e^{-i\varphi_{01}}\langle 1|. \end{aligned} \quad (30)$$

The left and right eigenvectors fulfill the biorthonormal condition  $\langle i_l|j_r\rangle_I = \delta_{i,j}$  [23].

Initially ( $t = t_i$ ) the eigenvectors of the open system [Eq. (30)] coincide with the eigenvectors of the closed



system [Eq. (17)], and hence the initial state of the closed system is also the initial state of the open system

$$|\psi_i\rangle_I = C_{D_1}(t_i)|D_{1r}(t_i)\rangle_I + C_{D_2}(t_i)|D_{2r}(t_i)\rangle_I. \quad (31)$$

The adiabatic STIRAP evolution ensures that the system remains within the subspace spanned by  $\{|D_{1r}(t)\rangle_I, |D_{2r}(t)\rangle_I\}$ . Inserting Eq. (31) into the time-dependent Schrödinger equation gives a set of equations that can be solved numerically for  $C_{D_1}$  and  $C_{D_2}$ . Without loss of generality we write the solutions as

$$\begin{aligned} C_{D_1}(t) &= e^{-\Gamma_0\alpha(t)} e^{i\gamma_1(t)} C_{D_1}(t_i), \\ C_{D_2}(t) &= e^{-\Gamma_0\beta(t)} e^{i\gamma_2(t)} C_{D_2}(t_i), \end{aligned} \quad (32)$$

and expand the wave function as

$$\begin{aligned} |\psi(t)\rangle_I &= e^{-\Gamma_0\alpha(t)} e^{i\gamma_1(t)} C_{D_1}(t_i) |D_{1r}(t)\rangle_I \\ &+ e^{-\Gamma_0\beta(t)} e^{i\gamma_2(t)} C_{D_2}(t_i) |D_{2r}(t)\rangle_I. \end{aligned} \quad (33)$$

The two dark states each acquire a complex geometric phase composed by real ( $\gamma_1$  and  $\gamma_2$ ) and imaginary parts ( $\Gamma_0\alpha(t)$  and  $\Gamma_0\beta(t)$ ) parameterized by the dephasing rate,  $\Gamma_0$ . As an example we choose an initial state  $|\psi_i\rangle = |0\rangle$  and apply the pulse sequence in Fig. 2(b) with parameters leading to  $\theta_{01} = \frac{\pi}{8}$ ,  $\phi_{01} = \pi$  and  $\gamma_{D_1} = -\pi$  (see details in caption of Fig. 3). As discussed in Sec. III this evolution corresponds to the Hadamard gate, Eq. (24) for the closed system. In Fig. 3 we show the evolution of the phases as a function of time for different values of the

dephasing rate  $\Gamma_0$ . The real geometric phases  $\gamma_1$  (light grey) and  $\gamma_2$  (grey) are unaffected by the dephasing and their values are identical to the analytical result for the closed system [Eq. (21)], which are marked with crosses in Fig. 3. The exponents  $\alpha$  and  $\beta$  are also almost unaffected by the dephasing rate. The results for  $\Gamma_0\tau = 10^{-5}$  and  $\Gamma_0\tau = 10^{-3}$  (solid) are identical while increasing the dephasing to  $\Gamma_0\tau = 10^{-1}$  (dotted) gives only a small deviation. Experimentally dephasing rates can be kept below  $\Gamma_0\tau = 10^{-3}$  and for these values of  $\Gamma_0$ ,  $\alpha$  and  $\beta$  are unaffected by the dephasing rate and hence the imaginary part of the phases  $\Gamma_0\alpha$  and  $\Gamma_0\beta$  scales linear with the dephasing rate. It should be noted that the value of  $\alpha$  and  $\beta$  depend on the initial state while  $\gamma_1$  and  $\gamma_2$  are unaffected and equal to the values in the closed system case. Going back to the Schrödinger picture yields

$$\begin{aligned} |\psi(t)\rangle &= \frac{1}{\sqrt{N}} e^{-\Gamma_0(t-t_i)} |0\rangle\langle 0| [e^{-\Gamma_0\alpha} e^{i\gamma_1} C_{D_1}(t_i) |D_{1r}\rangle_I \\ &+ e^{-\Gamma_0\beta} e^{i\gamma_2} C_{D_2}(t_i) |D_{2r}\rangle_I], \end{aligned} \quad (34)$$

where the wave function was re-normalized (factor  $1/\sqrt{N}$ ) because the non-Hermitian Hamiltonian does not preserve the norm. In the  $\{|0\rangle, |1\rangle\}$ -basis an initial state in the Schrödinger picture  $|\psi_i\rangle = a_i|0\rangle + b_i|1\rangle$  is transferred to a final non-normalized state  $|\psi_f\rangle_{non-norm} = L|\psi_i\rangle = a_f|0\rangle + b_f|1\rangle$ , with

$$L = \begin{bmatrix} e^{i\gamma_2} \cos^2 \theta_{01} e^{-\Gamma_0\beta} + e^{i\gamma_1} \sin^2 \theta_{01} e^{-\Gamma_0\alpha} & \cos \theta_{01} \sin \theta_{01} e^{-i\varphi_{01}} (e^{i\gamma_1} e^{-\Gamma_0\alpha} - e^{i\gamma_2} e^{-\Gamma_0\beta}) \\ \cos \theta_{01} \sin \theta_{01} e^{i\varphi_{01}} (e^{i\gamma_1} e^{-\Gamma_0\alpha} - e^{i\gamma_2} e^{-\Gamma_0\beta}) & e^{i\gamma_2} \sin^2 \theta_{01} e^{-\Gamma_0\beta} + e^{i\gamma_1} \cos^2 \theta_{01} e^{-\Gamma_0\alpha} \end{bmatrix}. \quad (35)$$

The normalization constant,  $N = |C_{D_1}(t_i)|^2 e^{-2\Gamma_0\alpha} + |C_{D_2}(t_i)|^2 e^{-2\Gamma_0\beta}$ , depends on the initial state, and the final state reads  $|\psi_f\rangle = \frac{1}{\sqrt{N}} |\psi_f\rangle_{non-norm}$ . While the phases  $\gamma_1$  and  $\gamma_2$  are robust with respect to dephasing, the appearance of the imaginary phases, affects the population of the states. Figure 4 shows the evolution of the population of the four states ( $|0\rangle, |1\rangle, |e\rangle, |2\rangle$ ) with initial state  $|\psi_i\rangle = |0\rangle$  and the pulse sequence in Fig. 2(b) with parameters  $\theta_{01} = \pi/8$ ,  $\varphi_{01} = \pi$  and  $\gamma_{D_1} = -\pi$  (see detailed parameters in the caption of Fig. 4). In the closed system these parameters lead to an implementation of the Hadamard gate and hence final populations  $P_0 = \frac{1}{2}$  and  $P_1 = \frac{1}{2}$ . When we introduce dephasing  $|\psi_i\rangle = |0\rangle$  leads to final population found from the no-jump evolu-

tion [Eq. (35)]

$$\begin{aligned} P_0 &= \frac{(\cos^2 \theta_{01} e^{-\Gamma_0\beta} - \sin^2 \theta_{01} e^{-\Gamma_0\alpha})^2}{\sin^2 \theta_{01} e^{-2\Gamma_0\alpha} - \cos^2 \theta_{01} e^{-2\Gamma_0\beta}}, \\ P_1 &= \frac{(\sin \theta_{01} \sin \theta_{01} (e^{-\Gamma_0\beta} + e^{-\Gamma_0\alpha}))^2}{\sin^2 \theta_{01} e^{-2\Gamma_0\alpha} - \cos^2 \theta_{01} e^{-2\Gamma_0\beta}}. \end{aligned} \quad (36)$$

The deviation from the closed system case ( $P_0 = (\cos^2 \theta_{01} - \sin^2 \theta_{01})^2, P_1 = 4 \sin^2 \theta_{01} \cos^2 \theta_{01}$ ) is thus determined by the two imaginary geometric phases,  $\Gamma_0\alpha$  and  $\Gamma_0\beta$ . The values of  $\alpha$  and  $\beta$  are found by numerically solving the time-dependent Schrödinger equation. On the scale of Fig. 4 there is no deviation between the closed and the open system results for realistic dephasing rates.

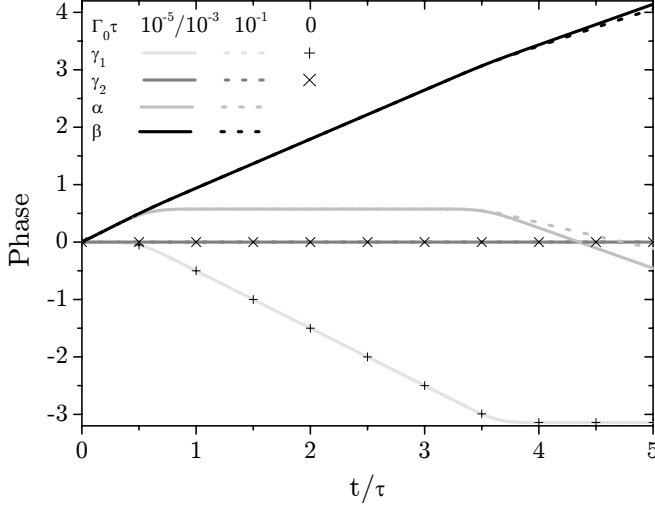


FIG. 3: Time evolution of  $\gamma_1$ ,  $\gamma_2$ ,  $\alpha$  and  $\beta$  for different dephasing rates,  $\Gamma_0$ . The calculations were made with  $\sin^2$  pulses (Eq. (6)) and all parameters are given in units of the pulse width,  $\tau$ :  $\varphi_2 = t/\tau$ ,  $A_{max,0}\tau/2\pi = 300$ ,  $A_{max,1} = A_{max,0}/(\sqrt{2} - 1)$ ,  $A_{max,2} = \sqrt{A_{max,0}^2 + A_{max,1}^2}$ ,  $\Delta t/\tau = 1$ , and  $\Delta T/\tau = \pi$ . These parameters lead to  $\theta_{01} = \frac{\pi}{8}$ ,  $\phi_{01} = \pi$  and  $\gamma_1 = -\pi$ . Dephasing rates  $\Gamma_0\tau = 10^{-5}$  and  $\Gamma_0\tau = 10^{-3}$  (solid) yield identical results, while  $\Gamma_0\tau = 10^{-1}$  (dotted) shows a small deviation at  $t/\tau \gtrsim 3.5$ .

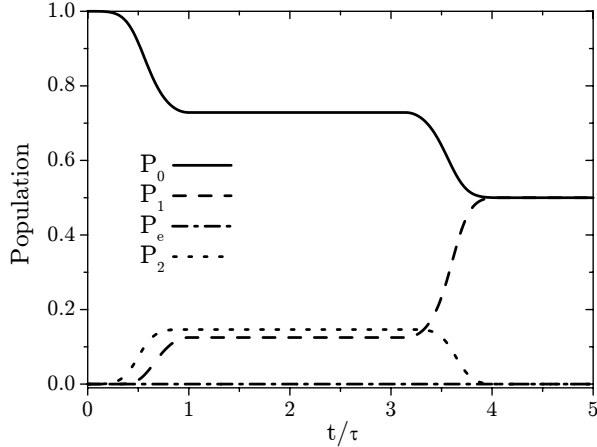


FIG. 4: Evolution of the population in the  $|0\rangle$ -state ( $P_0$ , solid), the  $|1\rangle$ -state ( $P_1$ , dashed), the  $|e\rangle$ -state ( $P_e$ , dashed-dotted) and the  $|2\rangle$ -state ( $P_2$ , dotted) with all population initially in the  $|0\rangle$ -state. The population evolve to  $P_0 = 1/2$  and  $P_1 = 1/2$  when no dephasing is present. With dephasing ( $\Gamma_0 T_0 = 10^{-3}$ ) the master equation as well as the no jump evolution [Eq. (35)] show no deviation from the no dephasing case on the scale of this figure. The calculations were made with  $\sin^2$  pulses [Eq. (6)] and all parameters are given in units of the pulse width,  $\tau$ :  $\varphi_2 = t/\tau$ ,  $A_{max,0}\tau/2\pi = 300$ ,  $A_{max,1} = A_{max,0}/(\sqrt{2} - 1)$ ,  $A_{max,2} = \sqrt{A_{max,0}^2 + A_{max,1}^2}$ ,  $\Delta t/\tau = 1$ , and  $\Delta T/\tau = \pi$ . These parameters lead to  $\theta_{01} = \frac{\pi}{8}$ ,  $\phi_{01} = \pi$  and  $\gamma_1 = -\pi$ .

## B. Jump evolution

For the present choice of parameters the system jumps in a small part of the Monte Carlo traces to the  $|0\rangle$ -state due to  $C_0 = \sqrt{2}\Gamma_0|0\rangle\langle 0|$ . If a jump occurs at  $t_j$  we expand the wave function ( $|0\rangle$ ) in the adiabatic basis of the instantaneous eigenstates

$$\begin{aligned} |\psi(t_j)\rangle &= |0\rangle \\ &= -\cos\theta_H(t_j)\sin\theta_{01}|D_{1r}(t_j)\rangle + \cos\theta_{01}|D_{2r}(t_j)\rangle \\ &\quad + \frac{1}{\sqrt{2}}\sin\theta_H(t_j)\sin\theta_{01}(|+_r(t_j)\rangle + |-_r(t_j)\rangle). \end{aligned} \quad (37)$$

After the jump the evolution is described by the no-jump non-Hermitian Hamiltonian [Eq. (28)]. In the adiabatic basis we can describe this evolution by calculating the geometric and dynamic phases acquired by the four states. The dark part of the wave function evolves as described for the no-jump evolution. The bright eigenstates ( $|+_r\rangle, |-_r\rangle$ ) are separated energetically from each other and from the dark states, such that there is no diabatic population transfer among these. The bright states acquire a dynamic phase as well as a complex geometric phase that can be calculated directly Eq. (3). The complex geometric phase is the same for the two bright states

$$\begin{aligned} \gamma_B &= i \int_{\bar{R}_i}^{\bar{R}_f} \langle \pm_l | \nabla_{\bar{R}} | \pm_r \rangle \cdot d\bar{R} \\ &= \frac{1}{2} i \Gamma_0 \sin^2\theta_{01} \int_{t_j}^t \sin^2\theta_H dt' - \frac{1}{2} \int_{t_j}^t \dot{\varphi}_2 \cos^2\theta_H dt' \\ &\equiv i\Gamma_0\delta + \gamma_b \end{aligned} \quad (38)$$

while the dynamic phase is different for the ( $|+_r\rangle, |-_r\rangle$ )-states

$$\vartheta_{\pm} = \mp \frac{1}{2} \int_{t_j}^t \sqrt{A_0^2 + A_1^2 + A_2^2} dt'.$$

The wave function at later times in the interaction picture is

$$\begin{aligned} |\psi(t)\rangle &= -\cos\theta_H(t_j)\sin\theta_{01}e^{-\Gamma_0\alpha}e^{i\gamma_1}|D_{1r}\rangle \\ &\quad + \cos\theta_{01}e^{-\Gamma_0\beta}e^{i\gamma_2}|D_{2r}\rangle \\ &\quad + \frac{1}{\sqrt{2}}\sin\theta_H(t_j)\sin\theta_{01}e^{-\Gamma_0\delta}e^{i\gamma_b}e^{i\vartheta_+}|+_r\rangle \\ &\quad + \frac{1}{\sqrt{2}}\sin\theta_H(t_j)\sin\theta_{01}e^{-\Gamma_0\delta}e^{i\gamma_b}e^{i\vartheta_-}|-_r\rangle. \end{aligned} \quad (39)$$

Going back to the Schrödinger picture and calculating the final populations in the atomic states yields

$$P_0 = \frac{1}{N} |\cos^2 \theta_{01} e^{-\Gamma_0 \beta} - \sin^2 \theta_{01} \cos \theta_H(t_j) e^{-\Gamma_0 \alpha} e^{i\gamma_1}|^2, \quad (40)$$

$$P_1 = \frac{1}{N} \sin^2 \theta_{01} \cos^2 \theta_{01} |e^{-\Gamma_0 \beta} + \cos \theta_H(t_j) e^{-\Gamma_0 \alpha} e^{i\gamma_1}|^2,$$

$$P_e = \frac{1}{N} \sin^2 \theta_{01} \sin^2 \theta_H(t_j) e^{-2\Gamma_0 \delta} \sin^2 \vartheta_-,$$

$$P_2 = \frac{1}{N} \sin^2 \theta_{01} \sin^2 \theta_H(t_j) e^{-2\Gamma_0 \delta} \cos^2 \vartheta_-,$$

where the normalization constant is given as  $N = \sin^2 \theta_{01} \cos^2 \theta_H(t_j) e^{-2\Gamma_0 \alpha} + \cos^2 \theta_{01} e^{-2\Gamma_0 \beta} + \sin^2 \theta_{01} \sin^2 \theta_H(t_j) e^{-2\Gamma_0 \delta}$ . Phases are only acquired from the latest jump time,  $t_j$ . The final populations can in this way be calculated after each Monte Carlo trace and the deviations from the closed system case can be explained by the complex geometric phases acquired by the adiabatic states. When all complex geometric phases are carefully taken into account an average over many traces reproduces the numerical solution of the master equation [Eq. (26)]. This is shown in Fig. 5, where we enlarge the last part of the evolution of the populations shown in Fig. 4. On this scale deviations between the closed and the open system are visible. The closed system (dash-dot-dot curves) yields final populations  $P_0 = 1/2$  and  $P_1 = 1/2$  as expected for the initial state  $|\psi_i\rangle = |0\rangle$  and the Hadamard gate applied (parameters are specified in the caption of Fig. 5). The evolution of the open system is determined either by solving the master equation (solid curves) or by the Monte Carlo method. The final populations predicted by the no-jump evolution (dashed curves) deviates from the master equation (solid curves) on the order of  $10^{-3}$ . An average over 10000 Monte Carlo traces (dash-dot-dash) reduces the deviation to an order of  $10^{-4}$ , while averaging over 200000 traces (dotted curves) reduces it further to an order of  $10^{-5}$ .

### C. Fidelity of Hadamard gate

The calculated Monte Carlo traces can be used to determine the fidelity of the Hadamard gate. For a given initial state  $|\psi_i\rangle$  we can determine the fidelity as the overlap between the target (closed-system) wave function  $|\psi_0\rangle$  and the final Monte Carlo wave functions (no jump  $|\psi_{nj}\rangle$  or one jump at  $t_j$   $|\psi_j(t_j)\rangle$ ) weighed by the probability of each trace (no jump  $P_{nj}$  or one jump  $P_j(t_j)$ ). The contributions to the fidelity from traces with more than one jump ( $F_{i,mj}$ ) is negligible for realistic dephasing rates.

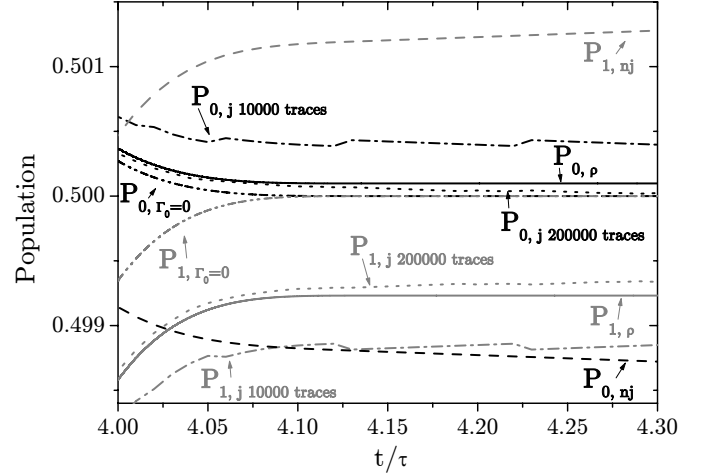


FIG. 5: Population in the  $|0\rangle$ -state ( $P_0$ , black), the  $|1\rangle$ -state ( $P_1$ , grey), when the system is not subject to dephasing ( $P_{i,\Gamma_0=0}$ , dot-dot-dash) as well as when dephasing ( $\Gamma_0\tau = 10^{-3}$ ) is present. The graph shows only the final part of the time evolution, where the differences can be distinguished. With dephasing the full curve ( $P_{i,\rho}$ ) shows the solution of the master equation [Eq. (25)], the dashed curve ( $P_{i,nj}$ ) the no-jump trace, while the last two curves are averages over 10000 ( $P_{i,j}$  10000 traces dash-dot-dash) and 200000 ( $P_{i,j}$  200000 traces, dotted) jump and no-jump traces. The calculations were made with  $\sin^2$  pulses (Eq. (6)) and all parameters are given in units of the pulse width,  $\tau$ :  $\varphi_2 = t/\tau$ ,  $A_{max,0}\tau/2\pi = 300$ ,  $A_{max,1} = A_{max,0}/(\sqrt{2}-1)$ ,  $A_{max,2} = \sqrt{A_{max,0}^2 + A_{max,1}^2}$ ,  $\Delta t/\tau = 1$ , and  $\Delta T/\tau = \pi$ .

The fidelity, accordingly reads

$$F_i = P_{nj} |\langle \psi_0 | \psi_{nj} \rangle|^2 + \int P_j(t_j) |\langle \psi_0 | \psi_j(t_j) \rangle|^2 dt_j + F_{i,mj} \quad (41)$$

$$= |\langle \psi_0 | \psi_{nj, non-norm.} \rangle|^2 + \int |\langle \psi_0 | \psi_{j, non-norm.}(t_j) \rangle|^2 dt_j + F_{i,mj},$$

where we use the non-normalized Monte Carlo wave functions to avoid calculating the probability distributions directly. As a first approximation the fidelity can be calculated neglecting the jump traces

$$F_{i,nj} = |\langle \psi_0 | \psi_{nj, non-norm.} \rangle|^2 = |\langle \psi_i U_0^\dagger | L \psi_i \rangle|^2 \quad (42)$$

$$= e^{-2\Gamma_0 \alpha_{nj}} |C_{D_1}(t_i)|^4 + e^{-2\Gamma_0 \beta_{nj}} |C_{D_2}(t_i)|^4$$

$$+ 2e^{-\Gamma_0(\alpha_{nj} + \beta_{nj})} |C_{D_1}(t_i)|^2 |C_{D_2}(t_i)|^2$$

$$\times \cos(\gamma_{1,nj} - \gamma_{2,nj} - \gamma_{D_1}).$$

The decrease in the fidelity is governed by the geometric phases acquired during the no-jump evolution. The non-normalized wave function for traces with one jump at the instant  $t_j$  is found in three steps. The system evolves under the non-Hermitian Hamiltonian until  $t_j$ ,  $|\psi_j(t_j)\rangle = L|\psi_j(t_i)\rangle$ , where it acquires geometric phases



$-\Gamma_0\alpha + i\gamma_1$  and  $-\Gamma_0\beta + i\gamma_2$ . At  $t_j$  the system jumps and  $|\psi_j(t_j)\rangle = \sqrt{2\Gamma_0}|0\rangle\langle 0|\psi_j(t_j)\rangle$ . Finally the system evolves under the non-Hermitian Hamiltonian from  $t_j$  to  $t_f$ ,  $|\psi_j(t_f)\rangle = L|\psi_j(t_j)\rangle$ , where it acquires geometric phases  $-\Gamma_0\alpha' + i\gamma_1'$  and  $-\Gamma_0\beta' + i\gamma_2'$ . The fidelity from the jump traces will hence be proportional to  $\sqrt{2\Gamma_0}^2$

$$F_i = F_{i,nj} + 2\Gamma_0 \int \xi_{i,j}(\alpha, \gamma_1, \alpha', \gamma_1', \beta, \gamma_2, \beta', \gamma_2') dt_j, \quad (43)$$

where  $\xi_{i,j}(\alpha, \gamma_1, \alpha', \gamma_1', \beta, \gamma_2, \beta', \gamma_2')$  is determined by the geometric phases in the jump traces with jump at  $t_j$ . Traces with more than one jump will contribute with terms proportional to higher orders of  $\Gamma_0$  and are therefore neglected. The fidelity determined from the Monte Carlo traces can be compared with the Uhlmann state fidelity calculated from the final closed system density matrix  $\rho_0$  and the final open system density matrix  $\rho(\Gamma_0)$  [24]

$$F_{\rho,i} = \left( \text{Tr} \sqrt{\rho_0^{1/2} \rho(\Gamma_0) \rho_0^{1/2}} \right)^2. \quad (44)$$

Both  $F_i$  and  $F_{\rho,i}$  give the fidelity for a given initial state. The average fidelity can be found by integrating over the surface of the Bloch sphere

$$F = \frac{1}{4\pi} \int F_i d\Omega. \quad (45)$$

This averaging procedure can be simplified to only averaging over the six axial pure initial states on the Bloch sphere,  $\Lambda = \{|0\rangle, |1\rangle, \frac{1}{\sqrt{2}}(|0\rangle + |1\rangle), \frac{1}{\sqrt{2}}(|0\rangle - |1\rangle), \frac{1}{\sqrt{2}}(|0\rangle + i|1\rangle), \frac{1}{\sqrt{2}}(|0\rangle - i|1\rangle)\}$  [25]

$$F = \frac{1}{6} \sum_{|\psi_i\rangle \in \Lambda} F_i. \quad (46)$$

In Fig. 6 we show the average fidelity as a function of the dephasing rate by the Monte Carlo method when only no-jump traces are taken into account (solid, black curve) and when traces with no or one jump are included (dotted, black curve). These are compared with the full master equation solution (dashed, grey curve). The fidelities are all calculated for the Hadamard gate implemented by the parameters  $\theta_{01} = \pi/8$ ,  $\varphi_{01} = \pi$  and  $\gamma_{D1} = -\pi$  as in all previous numerical results. The fidelity decreases as expected when the dephasing rate increases, but is still acceptable when the system is subject to realistic dephasing rates. The no-jump results gives a lower bound on the fidelity but it is necessary to include traces with one jump in order to get a satisfactory accuracy for realistic dephasing rates. Eq. (42) shows explicitly how the no-jump fidelity depends on the geometric phases acquired during the no-jump evolution.

## V. SUMMARY AND CONCLUSION

We presented a method to describe the adiabatic evolution of an open system using the quantum Monte Carlo

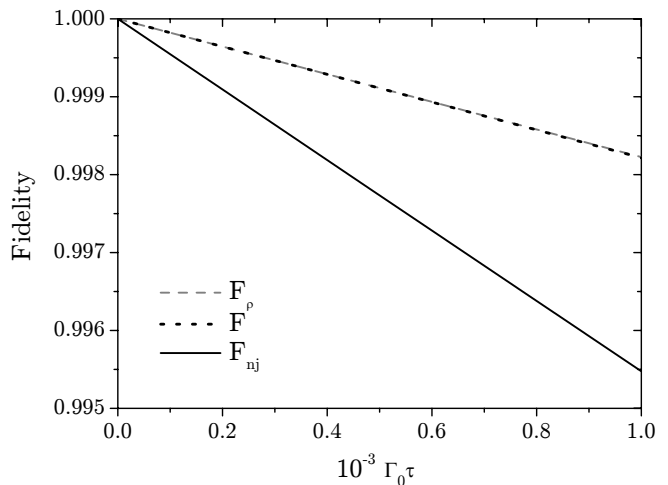


FIG. 6: Fidelity as a function of the dephasing rate,  $\Gamma_0$ . The dashed grey curve shows the density matrix calculation,  $F_\rho$  [Eq. (44)], the dotted black curve the Monte Carlo calculation including traces with no jump as well as one jump ( $F$ ) and solid black includes only no-jump traces ( $F_{nj}$ ) [Eq. 42]. The calculations were made with  $\sin^2$  pulses [Eq. (6)] and all parameters are given in units of the pulse width,  $\tau$ :  $\varphi_2 = t/\tau$ ,  $A_{max,0}\tau/2\pi = 300$ ,  $A_{max,1} = A_{max,0}/(\sqrt{2} - 1)$ ,  $A_{max,2} = \sqrt{A_{max,0}^2 + A_{max,1}^2}$ ,  $\Delta t/\tau = 1$ , and  $\Delta T/\tau = \pi$ .

method and keeping track of all acquired phases. This method has the advantage that it reveals the evolution of the single quantum trajectories and discloses the geometric or dynamic nature of the acquired phases in the adiabatic basis. We considered a tripod system with three laser fields applied and calculated its instantaneous adiabatic eigenstates. The tripod system is subject to a double STIRAP process and during this the adiabatic eigenstates acquire complex geometric phases. In the closed system case the geometric phases are purely real ( $\gamma_{D1}$ ) and all population is at all times in the two dark (with zero energy eigenvalues) adiabatic eigenstates. The acquired geometric phases create a phase difference between the two dark states and hence generate a rotation in the atomic  $\{|0\rangle, |1\rangle\}$ -basis. With the right parameter choice this rotation implements the Hadamard gate, which we have used as an example in the numerical simulations.

When dephasing is present we used the quantum Monte Carlo method, where the system either follow a non-Hermitian no-jump evolution during the whole time sequence or at one or more instants of time jump to the  $|0\rangle$ -state. Before, in between and after jumps the system follows the non-Hermitian no-jump evolution. During the non-Hermitian evolution the instantaneous adiabatic eigenstates acquire complex geometric phases. These deviate from the closed system case mainly because they contain non-negligible imaginary parts, which lead to a decay of the adiabatic eigenstates and hence influence the populations resulting in imperfect gate performance.

The specific Hadamard gate simulations show that the fidelity is still appreciable at realistic dephasing rates.

### Acknowledgments

This work is supported by the Danish Research Agency (Grant. No. 2117-05-0081).

- 
- [1] M. V. Berry, Proc. R. Soc. London, Ser. A **392**, 45 (1984).  
 [2] D. Ellinas and J. Pachos, Phys. Rev. A **64**, 022310 (2001).  
 [3] P. Solinas, P. Zanardi, and N. Zanghi, Phys. Rev. A **70**, 042316 (2004).  
 [4] I. Fuentes-Guridi, F. Girelli, and E. Livine, Phys. Rev. Lett. **94**, 020503 (2005).  
 [5] S. L. Zhu and P. Zanardi, Phys. Rev. A **72**, 020301 (2005).  
 [6] E. Sjöqvist, Acta Phys. Hung. B **26**, 195 (2006).  
 [7] S. Dasgupta and D. A. Lidar, J. Phys. B **40**, S127 (2007).  
 [8] K. Mølmer, Y. Castin, and J. Dalibard, J. Opt. Soc. Am. B **10**, 524 (1993).  
 [9] K. Mølmer and Y. Castin, Quantum Semiclass.Opt. **8**, 49 (1996).  
 [10] K. Bergmann, H. Theuer, and B. W. Shore, Rev. Mod. Phys. **70**, 1003 (1998).  
 [11] A. Messiah, *Quantum Mechanics*, vol. 2 (North-Holland publishing company, 1961).  
 [12] R. G. Unanyan, B. W. Shore, and K. Bergmann, Phys. Rev. A **59**, 2910 (1999).  
 [13] U. Gaubatz, P. Rudecki, S. Schiemann, and K. Bergmann, J. Chem. Phys. **92**, 5363 (1990).  
 [14] B. Broers, H. B. van Linden van den Heuvell, and L. D. Noordam, Phys. Rev. Lett. **69**, 2062 (1992).  
 [15] L. S. Goldner, C. Gerz, R. J. C. Spreeuw, S. L. Rolston, C. I. Westbrook, W. D. Phillips, P. Marte, and P. Zoller, Phys. Rev. Lett. **72**, 997 (1994).  
 [16] J. L. Sørensen, D. Møller, T. Iversen, J. B. Thomsen, F. Jensen, P. Staantum, D. Voigt, and M. Drewsen, New J. Phys. **8**, 261 (2006).  
 [17] T. Cubel, B. K. Teo, V. S. Malinovsky, J. R. Guest, A. Reinhard, B. Knuffman, P. R. Berman, and G. Raithel, Phys. Rev. A **72**, 023405 (2005).  
 [18] J. Lawall and M. Prentiss, Phys. Rev. Lett. **72**, 993 (1994).  
 [19] D. Møller, L. B. Madsen, and K. Mølmer, Phys. Rev. A **75**, 062302 (2007).  
 [20] F. Wilczek and A. Zee, Phys. Rev. Lett. **52**, 2111 (1984).  
 [21] S. Haroche and J.-M. Raimond, *Exploring the Quantum* (Oxford University Press, Oxford, 2006), chapter 4.  
 [22] J. C. Garrison and E. M. Wright, Phys. Lett. A **128**, 177 (1988).  
 [23] F. H. M. Faisal, *Theory of multiphoton processes* (Plenum Press, New York, 1987), chapter 11.2.  
 [24] A. Uhlmann, Rep. Math. Phys. **9**, 273 (1976).  
 [25] M. D. Bowdrey, D. K. L. Oi, A. J. Short, K. Banaszek, and J. A. Jones, Phys. Lett. A **294**, 258 (2002).